ACS NANO

www.acsnano.org

ARTICLE

Dynamic, Spontaneous Blistering of Substrate-Supported Graphene in Acidic Solutions

Yunqi Li, Bowen Wang, Wan Li, and Ke Xu*

Cite This: https://doi.org/10.1021/acsnano.1c11616

Read Online

ACCESS | Metrics & More | Article Recommendations | Supporting Information

ABSTRACT: We report that for monolayer and few-layer graphene on common silicon and glass substrates, acidic solutions induce fast, spontaneous generation of solution-enclosing blisters/bubbles. Using interference reflection microscopy, we monitor the blister-generating process *in situ* and show that at pH < ~2, nanoscale to micrometer-sized graphene blisters, up to ~100 nm in height, are universally generated with high surface coverages on hydrophilic, but not hydrophobic, surfaces. The spontaneously generated blisters are highly dynamic, with growth, merging, and reconfiguration occurring at second-to-minute time scales. Moreover, we show that in this dynamic system, graphene behaves as a semipermeable membrane that allows the relatively free passing of water, impeded passing of the NaCl solute, and no passing of large dye molecules. Consequently, the blister volumes can be fast and reversibly modulated by the solution osmotic pressure.

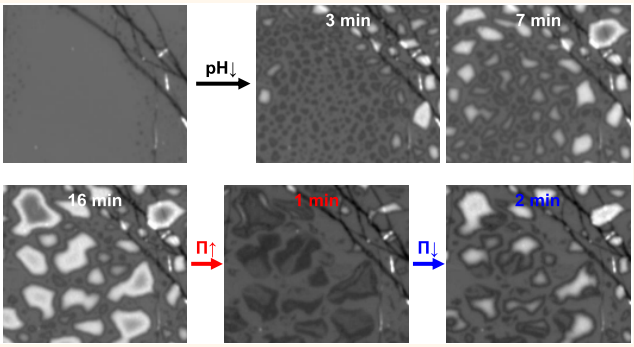

KEYWORDS: *graphene blister, graphene−substrate interaction, graphene semipermeable membrane, graphene defects, graphene in acids, in situ microscopy*

The outstanding electrical and optical properties of graphene are intricately linked to its extraordinary mechanical behaviors.[1−3] In particular, for substrate-supported graphene, a common device geometry, the formation of gas- or liquid-enclosing bubbles/blisters[4] has in recent years attracted substantial research interest[5−13] for understanding the properties of graphene itself and graphene−substrate interactions, the confinement of molecules,[14−18] and potential applications. Whereas the controlled formation and modulation of bubbles are attainable with carefully engineered substrate geometries,[5,7−9] less control has been achieved for the generation of bubbles/blisters for graphene deposited on common, unpatterned substrates,[4,6,10−13] and when formed, the structures are often static at the hour time scales. Separately, the notion that graphene, after proper processing, may behave as a semipermeable membrane for the selective passing of molecules has garnered focused attention over the past decade.[8,19−25]

In this work, we report the unexpected discovery that for graphene deposited on common silicon and glass substrates the application of acidic solutions of pH< ~2 leads to the fast, spontaneous generation of solution-enclosing blisters with high surface coverages. Initially appearing as nanoscale bubbles across the substrate at high densities, within minutes the blisters dynamically coalesce to several micrometers in size and ~100 nm in height. Intriguingly, we further show that in this dynamic system graphene behaves as a semipermeable membrane, so that the blister volumes can be fast modulated by the solution osmotic pressure in a reversible fashion.

RESULTS AND DISCUSSION

Interference Reflection Microscopy (IRM) Unveils Dynamic, Spontaneous Blistering of Graphene on the Glass Surface. Figure 1a presents the typical sample geometry for our *in situ* monitoring of graphene morphology. Monolayer graphene was deposited on a transparent substrate and then submerged in an aqueous top medium that was readily exchanged during the experiment. An index-matched oil-

Received: December 30, 2021
Accepted: March 17, 2022

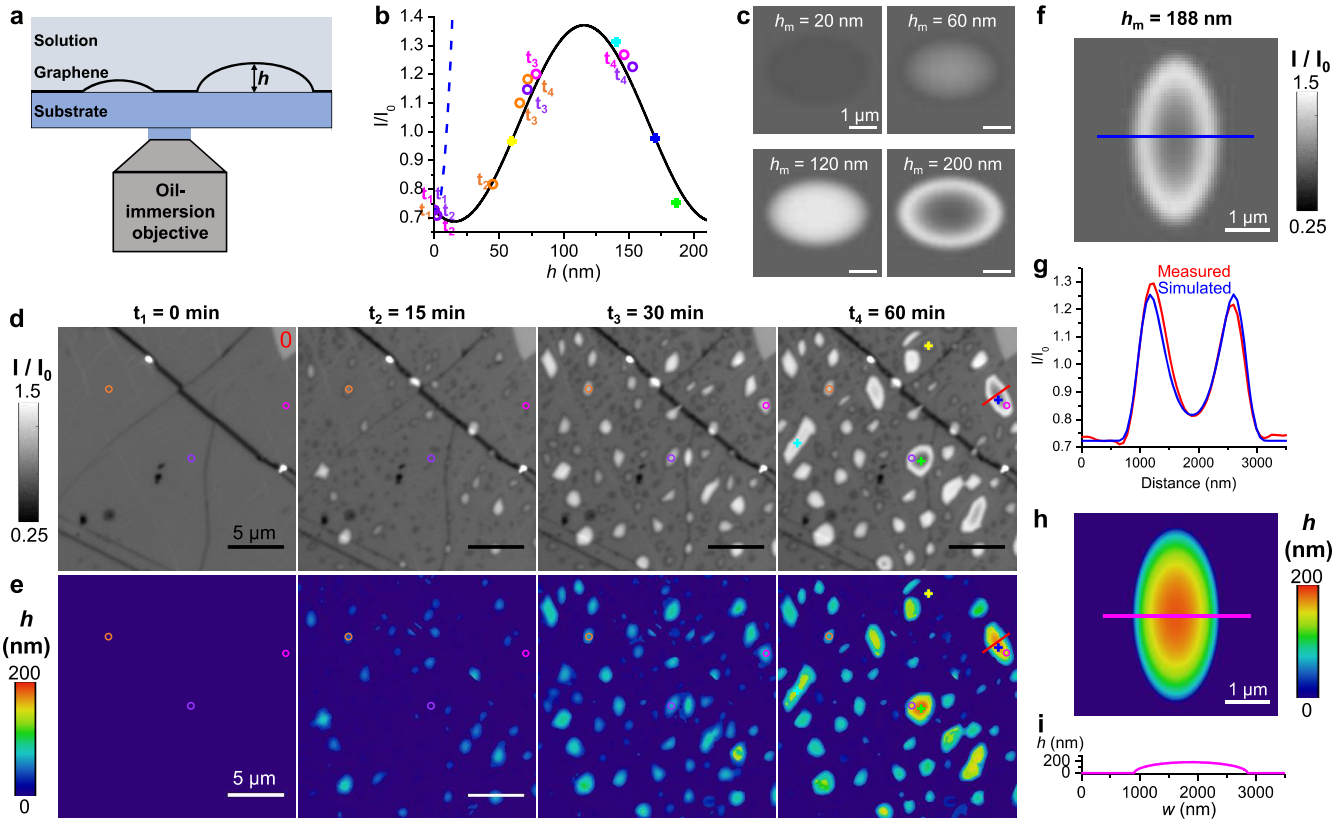

Figure 1. IRM unveils dynamic, spontaneous blistering of graphene on the glass surface. (a) Schematic of the system. (b) Predicted IRM signal (light intensity I normalized by the intensity at the bare substrate I_0) for monolayer graphene on glass, as a function of the local blister height h, for blisters enclosing an aqueous solution (back line) *vs* gas (blue dashed line). (c) Simulated IRM images of solution-enclosed graphene blisters of varying maximal heights h_m. (d) Experimental *in situ* IRM images for monolayer graphene on a glass surface, in 0.1 M HCl for different amounts of time. "0" marks locally exposed glass surface. (e) Converted blister height maps. Colored crosses (for final time point) and circles (for different time points): locations for which the IRM signal in (d) is plotted in (b) against the inferred height in (e). Slight value shifts are due to smoothing of the spatiotemporal signals in data processing. (f) Simulated IRM image for a blister of h_m = 188 nm, which matched well to the experimental data for the blister crossed by the red line in the last time point in (d). (g) Overlay of the simulated and measured IRM signals along the blue and red lines in (f) and (d), respectively. (h) Heightmap of the simulated data in (f). (i) Height profile along the magenta line in (h), shown at a 1:1 scale for width w and height h.

immersion objective lens imaged through the substrate in the mode of IRM. While originally developed for cell imaging,[26,27] we recently established IRM as a powerful tool for the quantitative, *in situ* imaging of graphene structures, defects, and reactions.[28−32]

Unexpectedly, for graphene deposited on common glass coverslips, as we replaced the top medium of water with 0.1 M HCl, within minutes, we observed the generation of numerous nanoscale features of varying IRM contrasts that were distributed across the sample at high densities (Figure 1d). While generally growing bigger with increased IRM contrasts at the ∼10 min time scale, these nanoscale structures also showed dynamic merging and reconfigurations, so that they gradually coalesced into micrometer-sized islands (Figure 1d, Figure S1, and Movie S1). As we examined similarly treated samples on different days, we consistently observed the high coverage of comparable islands (Figure S1).

As the system involved only an HCl solution and the island edges exhibited gradual changes in IRM signal, we reasoned that the islands were graphene blisters/bubbles[4] that locally delaminated from the glass surface (schematic in Figure 1a) and hence altered the IRM signal, rather than surface depositions as we previously examined for other systems.[31] Yet, the spontaneous formation of these blisters on the flat glass surface differs from previous experiments in which engineered substrate geometries are employed to induce bubbles.[5,7−9] Meanwhile, the dynamic nature of these blisters further contrasts with the relatively static bubbles and surface adlayers trapped between graphene and substrates reported in previous studies.[4,6,10−18,33−35] Instead, here graphene started as a regular, flat layer stable on the glass surface, yet the introduction of 0.1 M HCl induced the fast, spontaneous generation of blisters, and such blisters rearranged dynamically over time.

Theoretical modeling (Methods and Supporting Information) showed that if we assumed that the blisters enclosed aqueous solutions, the IRM readout, as presented as local light intensity I divided by the intensity at a direct substrate−solution interface I_0 (I/I_0), would initially drop from ∼0.75 to 0.69 as the blister height increases to ∼15 nm (Figure 1b). Subsequently, the signal would rapidly rise to ∼1.37 as the blister height increases to ∼115 nm, when the signal would drop again with further blister growth (Figure 1b). As we examined the IRM signal time traces of different growing blisters, we observed trends consistent with the above-predicted bounds (Figure S2). In contrast, if the blisters enclosed gas, theory predicts that the IRM signal I/I_0 would rise dramatically, reaching ∼28 at a blister height of ∼130 nm

https://doi.org/10.1021/acsnano.1c11616
ACS Nano XXXX, XXX, XXX−XXX

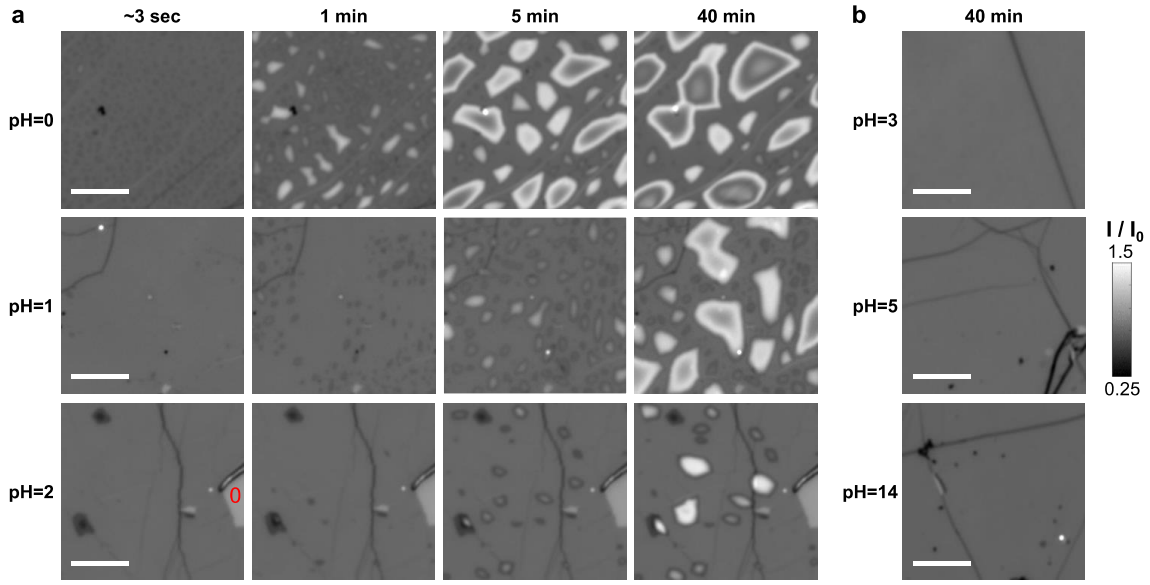

Figure 2. pH dependence of blister generation for graphene on the glass surface. (a) *In situ* IRM images of monolayer graphene on glass submerged in pH = 0, pH = 1, and pH = 2 HCl solutions, at different time points. (b) IRM images for similar samples after 40 min of immersion in a pH = 3 HCl solution, pH ~5 Milli-Q water, and a pH = 14 NaOH solution. Scale bars: 5 μm.

before the signal bounces back (Figure S2), drastically different from our experimental observations. Simulated IRM images of solution-enclosed graphene blisters of varying maximal heights, accounting for the diffraction-limited optical resolution, further showed good agreement with the experimental data (Figure 1c,f–h and Figure S3).

Thus, our IRM data indicate the spontaneous generation of blisters enclosing aqueous solutions between the graphene monolayer and the substrate. To further examine this possibility, we removed the top solution as we continued recording IRM images (Figure S4). The originally bright blister features turned dark with low I/I_0 values, as expected for solution-enclosed graphene exposed to air (Figure S4). The blisters quickly shrank and disappeared within seconds, indicating fast evaporation of the nanoscopic water. This dynamic behavior again contrasts with the relative static graphene-trapped bubbles and surface adlayers noted in previous studies.[4,6,10−18,33−35] We further found that after the blisters were equilibrated with a NaCl solution, they shrank much slower in the air and maintained finite volumes over 30 min (Figure S4). This observation suggests that when the solute cannot evaporate, the blisters retain a concentrated solution in equilibrium with the ambient water vapor. Together, our results indicated that the blisters enclosed the applied solutions in the experiment.

By following the time traces and comparing them with our prediction in Figure 1b, we converted the IRM data into local height maps of the blisters (Figure 1e and Figure S1). This showed that the blisters grew to heights of ~50 nm in 15 min, ~100 nm at 30 min, and up to ~200 nm at 60 min. The bases of the blisters also grew wider over time to up to a few micrometers. Thus, the blisters were still quite flat, as illustrated by the cross section in Figure 1i. Plotting the height *versus* radius of different blisters showed a positive correlation with a slope of ~0.09 (Figure S1). This aspect ratio is comparable to previous liquid-trapped graphene bubbles/blisters on substrates.[10,12]

We further examined the behavior of few-layer graphene, utilizing the occasionally found multilayer islands in our dominantly monolayer samples (Figure S5). Interestingly, upon acid treatments, blisters were also generated between the multilayers and the substrate, and they were often larger than those at monolayers. This result may be linked to previous findings that the substrate adhesion energy of graphene is ~50% stronger for the monolayer than multilayers.[7]

Spontaneous Graphene Blistering Occurs under Acidic Conditions. To understand what factors led to the above fast spontaneous generation of blisters, we examined graphene samples in HCl solutions of different concentrations (Figure 2, Figure S6, and Movie S2). We thus found that when compared to the above-discussed blister dynamics in the 0.1 M HCl (pH = 1) solution at the ~10 min time scales, 1 M HCl (pH = 0) led to the instantaneous generation of nanoscale blisters at high densities in seconds, which grew rapidly and coalesced with each other in ~1 min, so that at 5 min, the system stabilized toward big blisters a few micrometers in lateral size and ~200 nm in height (Figure 2a). In contrast, in the 0.01 M HCl (pH = 2) solution, the generation of blisters was substantially slower and less abundant (Figure 2a). The pH = 3 and 5 solutions generated no blisters over 40 min (Figure 2b). We also compared results with pH < 1 H_2SO_4 and *p*-toluenesulfonic acid solutions and similarly observed blister generation (Figure S7). Meanwhile, a pH ~5 solution of Na_2SO_4 and basic conditions with 0.1 M (pH = 13) and 1 M (pH = 14) NaOH solutions did not produce graphene blisters (Figure 2b and Figure S7). Thus, graphene blisters are induced under acidic conditions of pH < ~2.

Spontaneous Graphene Blistering Occurs on Hydrophilic, but Not Hydrophobic, Substrates. We next investigated the effects of the substrate. The as-received glass coverslips, which we used above after sonication in isopropanol and water, were hydrophilic. After treating the coverslips with a piranha solution (1:3 H_2O_2/H_2SO_4), the surface became highly hydrophilic, and we observed a similar fast generation of graphene blisters on this substrate in 0.1 M HCl (Figure 3a).

https://doi.org/10.1021/acsnano.1c11616
ACS Nano XXXX, XXX, XXX−XXX

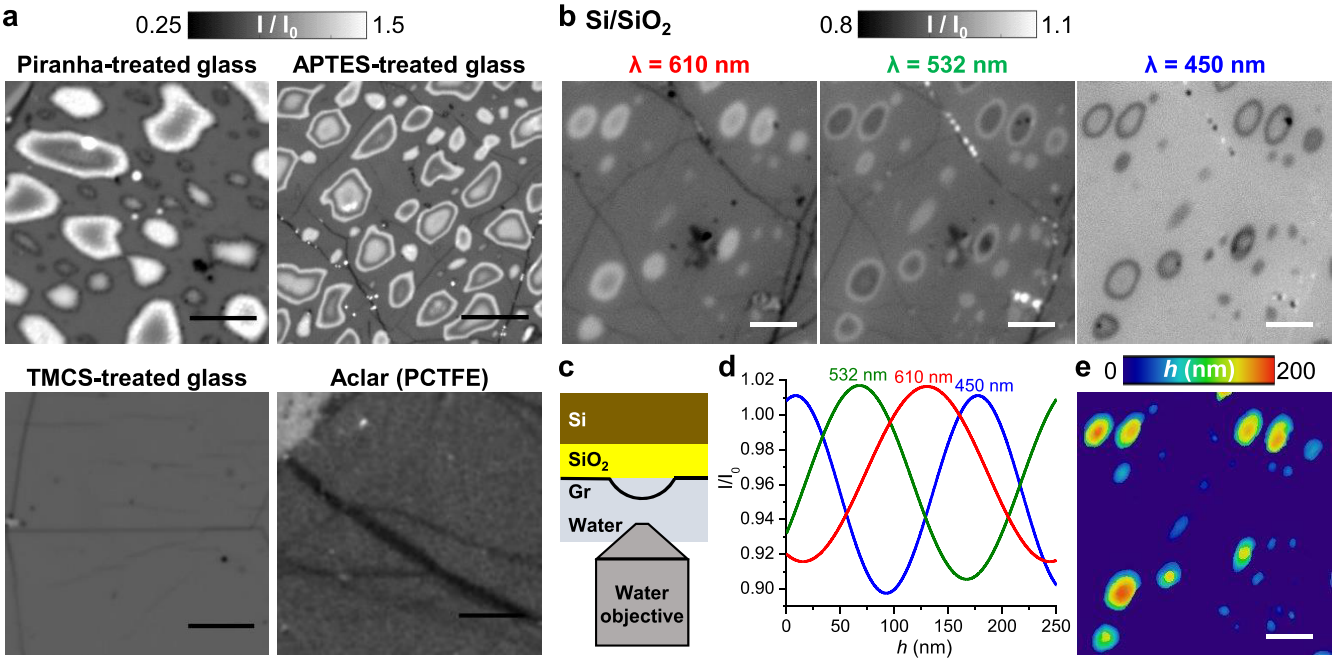

Figure 3. Spontaneous graphene blistering on different substrates. Monolayer graphene was deposited on different substrates and then immersed in 0.1 M HCl for ~1 h. (a) IRM images for graphene on piranha-treated glass, APTES-treated glass, TMCS-treated glass, and Aclar (PCTFE) film. (b) Reflected light microscopy images of graphene on a Si wafer coated with a ~290 nm layer of thermally grown oxide, under 610, 532, and 450 nm illuminations. For both imaging modes, signals are presented as the local light intensity I divided by the intensity at the direct substrate–solution interfaces I_0. (c) Sample geometry for the reflected light microscopy of graphene on Si/SiO_2. (d) Predicted image signals at the three wavelengths as a function of the water-enclosed blister height h. (e) Blister height map converted from the images in (b). Scale bars: 5 μm.

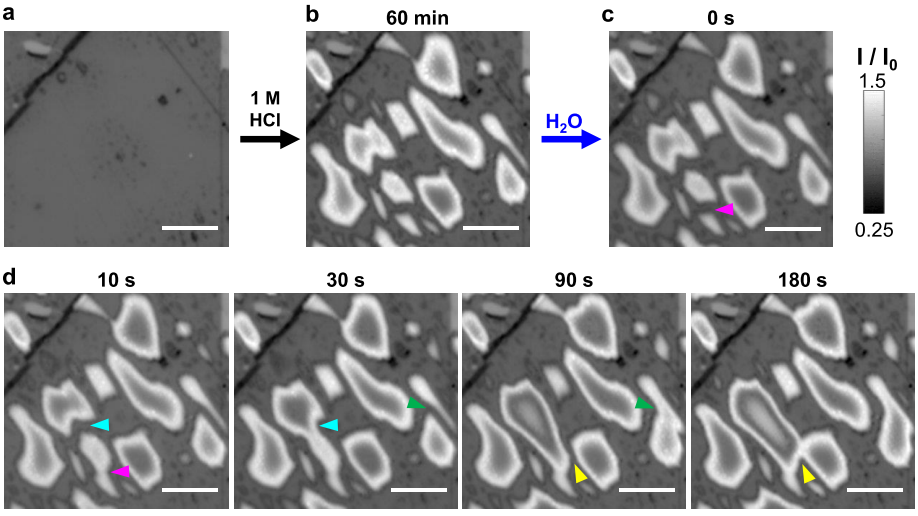

Figure 4. Fast expansion of blister volumes after changing the acid solution to water. (a, b) IRM images of monolayer graphene on glass, before (a) and after (b) immersing in 1 M HCl for 1 h. (c) The top solution was changed to Milli-Q water. (d) *In situ* IRM image sequences after different amounts of time, showing notable swelling of blisters. Colored arrowheads point to blister-merging events between the shown image sequences. Scale bars: 5 μm.

Functionalizing the glass surface with (3-aminopropyl)-triethoxysilane (APTES), which altered the hydrophilic glass surface from negatively charged to positively charged, did not affect the blister-generating capability (Figure 3a). In contrast, functionalizing the glass surface with chlorotrimethylsilane (TMCS), which yielded a hydrophobic surface, led to the full suppression of blisters in 0.1 M HCl (Figure 3a). Similarly, we found that for graphene deposited on the hydrophobic surface of polychlorotrifluoroethylene (PCTFE; Aclar) films, no blisters were generated (Figure 3a). Thus, blisters are generated for graphene deposited on hydrophilic but not hydrophobic surfaces. We also examined glass coverslips functionalized with trichloro(1*H*,1*H*,2*H*,2*H*-perfluorooctyl)-silane: the surface was both hydrophobic and oleophobic, onto which graphene did not adhere adequately but crumbled into sub-micrometer pieces (Figure S8).

We next examined the hydrophilic substrate of thermal oxide-coated silicon (Si/SiO_2) wafers, an often-used device

https://doi.org/10.1021/acsnano.1c11616
ACS Nano XXXX, XXX, XXX−XXX

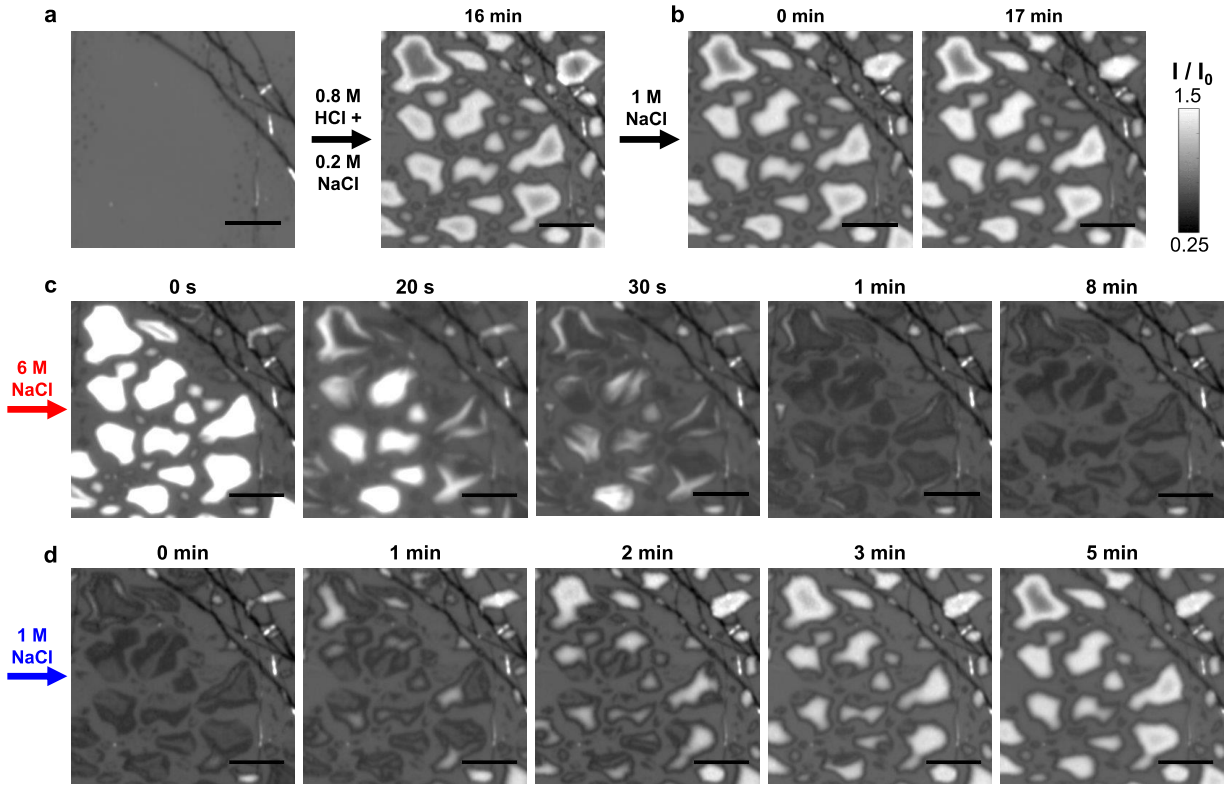

Figure 5. Reversible fast modulation of graphene blisters *via* solution osmotic pressure. (a) IRM images of monolayer graphene on glass, before (a) and after (b) immersing in a solution of 0.8 M HCl + 0.2 M NaCl for 16 min. (b) The top medium was changed to 1 M NaCl, with little changes in blister shapes observed over 17 min. (c) The top medium was next changed to 6 M NaCl, and IRM recorded a fast shrinkage of blister volumes. (d) The top medium was next reverted to 1 M NaCl, and IRM recorded a fast recovery of blister volumes. Scale bars: 5 μm.

substrate. As the substrate is opaque, we changed our imaging strategy, so that the sample was immersed in a 0.1 M HCl solution for ~1 h, rinsed with water, and then mounted upside-down for imagining with a water-immersion objective lens (Figure 3c). The resultant reflected light microscopy images visualized numerous blisters. Here, as the ~290 nm SiO_2 layer differently interfered with light of different wavelengths, we illuminated the sample at 610, 532, and 450 nm, respectively, and obtained images of varying contrasts (Figure 3b). Theory predicted different blister height-dependent signal evolution trends under the three wavelengths (Figure 3d). These predictions, as well as simulated blister images (Figure S9), matched well with our experimental observations (Figure 3b and Figure S9). We hence converted the triplex reflected-light micrograph into a heightmap, showing blisters up to ~200 nm in height (Figure 3e). Thus, comparable blisters were generated for graphene on the commonly used Si/SiO_2 substrate, although the dynamics are difficult to monitor *in situ* on this opaque substrate.

Graphene Blisters Are Quickkly Modulated by the Solution Osmotic Pressure as Graphene Acts as a Semipermeable Membrane. As we next examined the stability of the graphene blisters in different solutions, we found that the blisters expanded and shrank reversibly under different solute concentrations, and the behavior followed the osmotic pressure of the solution. Starting with blisters generated with 1 M HCl (Figure 4a,b), we found that as we replaced the sample solution with water, the blisters quickly expanded in volume at ~10 s time scales, so that the expanded blisters gradually merged with each other (arrowheads in Figure 4c,d).

To examine whether this dynamic behavior could be driven by changes in solute concentration and thus osmotic pressure, we examined a sample in which blisters were generated with a solution containing 0.8 M HCl and 0.2 M NaCl (Figure 5a). Replacing the top medium with an isotonic solution of 1 M NaCl did not notably alter the blisters over 17 min (Figure 5b). Next changing the medium to 6 M NaCl led to an initial flash of high IRM signal due to the high refractive index of the 6 M NaCl solution, yet the IRM signal then plummeted as the blister volumes shrank drastically in ~30 s (Figure 5c). Reverting the medium to 1 M NaCl led to rapid regrowth of the blisters, so that the system largely recovered the original blister volumes in ~3 min (Figure 5d).

The above results suggest that in our system the acid-treated graphene behaved as a semipermeable membrane[8,19−25] that more readily passed water molecules than the solute ions. Consequently, increased solute concentration and hence osmotic pressure of the solution withdrew water from the blisters to shrink their volumes, whereas decreased osmotic pressure of the solution drove more water into the blisters and induced blister expansion.

To further probe the semipermeable properties of the blisters, we next examined osmotic effects over longer time scales. Interestingly, as we applied 1 M NaCl to graphene blisters generated with 0.1 M HCl, whereas rapid shrinkage occurred at the second-to-minute time scale as water flew out under the higher osmotic pressure, the blisters gradually grew

https://doi.org/10.1021/acsnano.1c11616
ACS Nano XXXX, XXX, XXX−XXX

back after ~30 min (Figure S10). This result suggests the gradual diffusion of the NaCl solute into the blisters over the longer time scale. In contrast, as we added into the top medium the fluorescent dye sulforhodamine 101, fluorescence microscopy showed reduced sulforhodamine 101 signal at the graphene blisters, and this dye-exclusion effect was well maintained over 2 h (Figure S11). Together, our results indicated that the blisters allowed relatively free passing of water (~10 s time scales) and impeded passing of the NaCl solute (~10 min time scales), but effectively blocked the passing of the larger sulforhodamine 101 molecule.

CONCLUSION

In summary, with the exceptional contrast and *in situ* imaging capabilities offered by IRM, we discovered the fast, spontaneous generation of solution-enclosed blisters for graphene on common substrates. We thus showed that at pH < ~2 nanoscale to micrometer-sized graphene blisters, up to ~100 nm in height, were universally generated on hydrophilic surfaces, including the popular Si/SiO_2 substrates, but not on hydrophobic substrates. The blister-generation process was highly dynamic, with IRM-visualized growth, merging, and reconfiguration occurring at second-to-minute time scales, and we further showed that in such processes graphene behaved as a semipermeable membrane so that the blister volumes were readily modulated by the osmotic pressure of the solution.

Our intriguing observations may be explained below. Acidic conditions create atomic defects in graphene.[36,37] Raman spectroscopy (Figure S12) showed no noticeable generation of D peaks but enhanced hole doping after acid treatments, consistent with that expected from acid-induced defects and trapped water.[38−40] Thus, a moderate level of atomic defects creates a semipermeable membrane. Subsequently, if the substrate is hydrophilic, capillary action draws the aqueous solution into the narrow space between the graphene and substrate surfaces, hence initiating local delamination and dynamic reconfiguration of the inserted liquid to form blisters. The resultant blisters followed a height-to-radius aspect ratio of ~0.09, comparable to previous liquid-trapped graphene bubbles/blisters.[10,12] We further found the blisters to be larger at multilayers, a result attributable to the lower substrate adhesion of graphene multilayers than monolayers,[7] which likely facilitates local delamination. In contrast, a hydrophobic substrate disfavors water insertion and may more strongly bond the (relatively hydrophobic) graphene surface to prevent delamination, so blisters are not formed. Interestingly, we found that on the hydrophilic glass surface, chemical oxidated graphene no longer formed blisters (Figure S13), possibly because the oxidized graphene was more hydrophilic and thus adhered more strongly to the hydrophilic substrate.

As yet another demonstration of the power of IRM for *in situ* graphene characterization, our work highlights the dynamic nature of substrate-supported graphene, in terms of both its blister-forming capabilities and its semipermeable behavior. The observed spontaneous formation of blisters in acidic solutions further carries practical implications for understanding the stability of graphene devices under different operational conditions.

MATERIALS AND METHODS

Graphene Sample Preparation. For most samples, glass coverslips (#1.5, 50 × 24 mm, VWR, 16004-322) were cleaned by sonication in isopropanol for 10 min, followed by sonication in Milli-Q water for 10 min. For evaluating the behavior of different substrates (Figure 3) the following procedures were applied. For piranha treatment, coverslips were heated in a 1:3 H_2O_2/H_2SO_4 solution for 20 min and thoroughly rinsed with Milli-Q water. For APTES functionalization, the piranha-treated coverslips were immersed in a 10% (v/v) (3-aminopropyl)triethoxysilane (Sigma 440140) ethanol solution for 1 h. After that, the coverslips were rinsed with ethanol and Milli-Q water. For TMCS functionalization, the piranha-treated coverslips were placed in a chamber with chlorotrimethylsilane (Sigma 92361) vapor for 5 min. For trichloro(1*H*,1*H*,2*H*,2*H*-perfluorooctyl)silane functionalization, the piranha-treated coverslips were incubated in a chamber with trichloro(1*H*,1*H*,2*H*,2*H*-perfluorooctyl)silane (Fisher Scientific AAL1660609) vapor at 55 °C for 10 min. Aclar 33C (polychlorotrifluoroethylene) film of 0.2 mm thickness (Ted Pella) was cleaned by sonication in isopropanol for 10 min, followed by sonication in Milli-Q water for 10 min. Single-side-polished silicon wafers with a ~290 nm thermal oxide layer (Si/SiO_2; University Wafer) was piranha-treated and water-rinsed as above. CVD-grown graphene on copper foils (ACS Material or Graphene Supermarket) was spin-coated with a ~150 nm layer of poly(methyl methacrylate) (PMMA) and wet-transferred with a modified RCA cleaning process[41] onto the above substrates. PMMA was removed by immersion in acetone and isopropanol. Raman spectroscopy was performed with a Horiba LabRAM HR Evolution spectrometer with a 100× objective lens using 532 nm laser excitation and an 1800 lines/mm grating.

Optical Microscopy Characterizations. IRM, reflected light microscopy, and fluorescence microscopy were performed on an Olympus IX73 inverted epifluorescence microscope with a white light source (Olympus U-HGLGPS), as described previously.[28,42] IRM and fluorescence microscopy were performed using a UplanFl 100× oil-immersion objective (numerical aperture ~0.9 with iris diaphragm). Reflected light microscopy was performed using a UplanSapo 60× water-immersion objective (numerical aperture 1.2). For IRM and reflected light microscopy, the dichroic mirror position was mounted with a 50/50 beam splitter (Chroma 21000), and the emission filter position was left empty. For IRM, the excitation filter was D532/10x (Chroma). For reflected light microscopy, the excitation filter was FF01-610/5-25 (Semrock), D532/10x (Chroma), or FB450-10 (Thorlabs). For fluorescence microscopy, the excitation filter, dichroic mirror, and emission filter were ET545/25x (Chroma), zt561rdc-UF1 (Chroma), and ET605/70m (Chroma), respectively. For all microscopy modes, wide-field images were recorded using an Andor Zyla 4.2 sCMOS camera at ~10 frames per second with effective pixel sizes of 65 and 108 nm for the 100× and 60× objective lenses, respectively.

Theoretical Modeling of IRM and Reflected Light Microscopy Signals. Theoretical modeling of the IRM signal on transparent substrates, as well as reflected light microscopy signal on Si/SiO_2 substrates, was performed using the transfer-matrix method for thin films.[28,43] See details of theoretical derivations in the Supporting Information. For comparison with experiments, for IRM, the experimental signal I was first normalized by the signal measured at a direct substrate−solution interface (*e.g.*, locally exposed glass surface in the sample, as marked by "0" in Figure 1d), I_0. The resultant I/I_0 values were presented as images and compared with the theoretically predicted values (Figure 1b) to obtain the local blister height d_i and generate height maps. For reflected light microscopy, the experimental signal I, obtained at three fixed wavelengths of 610, 532, and 450 nm, was separately normalized by the signal measured at a direct water−substrate interface, I_0. The resultant I/I_0 values were presented as images. For each pixel, the I/I_0 values were compared with the theoretical values at the same three wavelengths for different local blister heights d_i (Figure 3d). Local d_i values were then assigned by minimizing the sum of the differences between the experimental and theoretical values at the three wavelengths.

Simulation of Blister IRM and Reflected Light Microscopy Images. Half-ellipsoids of varying heights were first simulated on grids 10 times finer than the actual pixel size. For simulating IRM

https://doi.org/10.1021/acsnano.1c11616
ACS Nano XXXX, XXX, XXX−XXX

images, the half-ellipsoids were converted from heights to IRM contrasts using the theoretically predicted IRM signal discussed above. The resultant simulated images were then spatially convolved with a 2D Gaussian function with an fwhm (full width at half-maximum) of 300 nm to simulate the diffraction-limited optical resolution. The images were then down-sampled to the actual pixel size to generate the final simulated IRM images. For graphene on Si/SiO_2, reflected light microscopy images were similarly simulated at the three experimental wavelengths.

ASSOCIATED CONTENT

Supporting Information

The Supporting Information is available free of charge at https://pubs.acs.org/doi/10.1021/acsnano.1c11616.

Detailed theoretical modeling of IRM and reflected light microscopy signals and supplementary figures containing additional experimental data and simulations under different experimental conditions (PDF)

Movie of *in situ* IRM images and converted height maps (MP4)

Movie of *in situ* IRM images at different pH values (MP4)

AUTHOR INFORMATION

Corresponding Author

Ke Xu − *Department of Chemistry, University of California, Berkeley, California 94720, United States;* orcid.org/0000-0002-2788-194X; Email: xuk@berkeley.edu

Authors

Yunqi Li − *Department of Chemistry, University of California, Berkeley, California 94720, United States;* orcid.org/0000-0001-8794-9910

Bowen Wang − *Department of Chemistry, University of California, Berkeley, California 94720, United States*

Wan Li − *Department of Chemistry, University of California, Berkeley, California 94720, United States;* orcid.org/0000-0001-5751-3550

Complete contact information is available at: https://pubs.acs.org/10.1021/acsnano.1c11616

Notes

The authors declare no competing financial interest.

ACKNOWLEDGMENTS

We thank Matthew Erodici (Kwabena Bediako Group) for help with Raman spectroscopy. This work was supported by STROBE, a National Science Foundation Science and Technology Center under Grant No. DMR 1548924, and the Bakar Fellows Award.

REFERENCES

(1) Papageorgiou, D. G.; Kinloch, I. A.; Young, R. J. Mechanical properties of graphene and graphene-based nanocomposites. *Prog. Mater. Sci.* **2017**, *90*, 75−127.

(2) Dai, Z.; Liu, L.; Zhang, Z. Strain Engineering of 2D Materials: Issues and Opportunities at the Interface. *Adv. Mater.* **2019**, *31*, 1805417.

(3) Sun, Y. W.; Papageorgiou, D. G.; Humphreys, C. J.; Dunstan, D. J.; Puech, P.; Proctor, J. E.; Bousige, C.; Machon, D.; San-Miguel, A. Mechanical properties of graphene. *Appl. Phys. Rev.* **2021**, *8*, 021310.

(4) Sanchez, D. A.; Dai, Z.; Lu, N. 2D Material Bubbles: Fabrication, Characterization, and Applications. *Trends Chem.* **2021**, *3*, 204−217.

(5) Bunch, J. S.; Verbridge, S. S.; Alden, J. S.; van der Zande, A. M.; Parpia, J. M.; Craighead, H. G.; McEuen, P. L. Impermeable Atomic Membranes from Graphene Sheets. *Nano Lett.* **2008**, *8*, 2458−2462.

(6) Stolyarova, E.; Stolyarov, D.; Bolotin, K.; Ryu, S.; Liu, L.; Rim, K. T.; Klima, M.; Hybertsen, M.; Pogorelsky, I.; Pavlishin, I.; Kusche, K.; Hone, J.; Kim, P.; Stormer, H. L.; Yakimenko, V.; Flynn, G. Observation of Graphene Bubbles and Effective Mass Transport under Graphene Films. *Nano Lett.* **2009**, *9*, 332−337.

(7) Koenig, S. P.; Boddeti, N. G.; Dunn, M. L.; Bunch, J. S. Ultrastrong adhesion of graphene membranes. *Nat. Nanotechnol.* **2011**, *6*, 543−546.

(8) Koenig, S. P.; Wang, L.; Pellegrino, J.; Bunch, J. S. Selective molecular sieving through porous graphene. *Nat. Nanotechnol.* **2012**, *7*, 728−732.

(9) Boddeti, N. G.; Liu, X.; Long, R.; Xiao, J.; Bunch, J. S.; Dunn, M. L. Graphene blisters with switchable shapes controlled by pressure and adhesion. *Nano Lett.* **2013**, *13*, 6216−6221.

(10) Khestanova, E.; Guinea, F.; Fumagalli, L.; Geim, A. K.; Grigorieva, I. V. Universal shape and pressure inside bubbles appearing in van der Waals heterostructures. *Nat. Commun.* **2016**, *7*, 12587.

(11) Ghorbanfekr-Kalashami, H.; Vasu, K. S.; Nair, R. R.; Peeters, F. M.; Neek-Amal, M. Dependence of the shape of graphene nanobubbles on trapped substance. *Nat. Commun.* **2017**, *8*, 15844.

(12) Sanchez, D. A.; Dai, Z.; Wang, P.; Cantu-Chavez, A.; Brennan, C. J.; Huang, R.; Lu, N. Mechanics of spontaneously formed nanoblisters trapped by transferred 2D crystals. *Proc. Natl. Acad. Sci. U.S.A.* **2018**, *115*, 7884−7889.

(13) Dai, Z.; Hou, Y.; Sanchez, D. A.; Wang, G.; Brennan, C. J.; Zhang, Z.; Liu, L.; Lu, N. Interface-Governed Deformation of Nanobubbles and Nanotents Formed by Two-Dimensional Materials. *Phys. Rev. Lett.* **2018**, *121*, 266101.

(14) Xu, K.; Cao, P. G.; Heath, J. R. Graphene visualizes the first water adlayers on mica at ambient conditions. *Science* **2010**, *329*, 1188−1191.

(15) Lee, M. J.; Choi, J. S.; Kim, J.-S.; Byun, I.-S.; Lee, D. H.; Ryu, S.; Lee, C.; Park, B. H. Characteristics and Effects of Diffused Water Between Graphene and a SiO_2 Substrate. *Nano Res.* **2012**, *5*, 710−717.

(16) Kim, H. H.; Yang, J. W.; Jo, S. B.; Kang, B.; Lee, S. K.; Bong, H.; Lee, G.; Kim, K. S.; Cho, K. Substrate-Induced Solvent Intercalation for Stable Graphene Doping. *ACS Nano* **2013**, *7*, 1155−1162.

(17) Li, Q.; Song, J.; Besenbacher, F.; Dong, M. Two-dimensional material confined water. *Acc. Chem. Res.* **2015**, *48*, 119−127.

(18) Fu, Q.; Bao, X. Surface chemistry and catalysis confined under two-dimensional materials. *Chem. Soc. Rev.* **2017**, *46*, 1842−1874.

(19) Hu, S.; Lozada-Hidalgo, M.; Wang, F. C.; Mishchenko, A.; Schedin, F.; Nair, R. R.; Hill, E. W.; Boukhvalov, D. W.; Katsnelson, M. I.; Dryfe, R. A.; Grigorieva, I. V.; Wu, H. A.; Geim, A. K. Proton transport through one-atom-thick crystals. *Nature* **2014**, *516*, 227−230.

(20) O'Hern, S. C.; Boutilier, M. S.; Idrobo, J. C.; Song, Y.; Kong, J.; Laoui, T.; Atieh, M.; Karnik, R. Selective ionic transport through tunable subnanometer pores in single-layer graphene membranes. *Nano Lett.* **2014**, *14*, 1234−1241.

(21) Achtyl, J. L.; Unocic, R. R.; Xu, L.; Cai, Y.; Raju, M.; Zhang, W.; Sacci, R. L.; Vlassiouk, I. V.; Fulvio, P. F.; Ganesh, P.; Wesolowski, D. J.; Dai, S.; van Duin, A. C.; Neurock, M.; Geiger, F. M. Aqueous proton transfer across single-layer graphene. *Nat. Commun.* **2015**, *6*, 6539.

(22) Huang, L.; Zhang, M.; Li, C.; Shi, G. Graphene-Based Membranes for Molecular Separation. *J. Phys. Chem. Lett.* **2015**, *6*, 2806−2815.

(23) Wang, L.; Drahushuk, L. W.; Cantley, L.; Koenig, S. P.; Liu, X.; Pellegrino, J.; Strano, M. S.; Bunch, J. S. Molecular valves for controlling gas phase transport made from discrete angstrom-sized pores in graphene. *Nat. Nanotechnol.* **2015**, *10*, 785−790.

(24) Wang, L.; Boutilier, M. S. H.; Kidambi, P. R.; Jang, D.; Hadjiconstantinou, N. G.; Karnik, R. Fundamental transport mechanisms, fabrication and potential applications of nanoporous atomically thin membranes. *Nat. Nanotechnol.* **2017**, *12*, 509−522.
(25) Chaturvedi, P.; Vlassiouk, I. V.; Cullen, D. A.; Rondinone, A. J.; Lavrik, N. V.; Smirnov, S. N. Ionic Conductance through Graphene: Assessing Its Applicability as a Proton Selective Membrane. *ACS Nano* **2019**, *13*, 12109−12119.
(26) Curtis, A. S. G. The mechanism of adhesion of cells to glass: A study by interference reflection microscopy. *J. Cell Biol.* **1964**, *20*, 199−215.
(27) Verschueren, H. Interference reflection microscopy in cell biology: Methodology and applications. *J. Cell Sci.* **1985**, *75*, 279−301.
(28) Li, W.; Moon, S.; Wojcik, M.; Xu, K. Direct optical visualization of graphene and its nanoscale defects on transparent substrates. *Nano Lett.* **2016**, *16*, 5027−5031.
(29) Wojcik, M.; Li, Y.; Li, W.; Xu, K. Spatially resolved *in situ* reaction dynamics of graphene via optical microscopy. *J. Am. Chem. Soc.* **2017**, *139*, 5836−5841.
(30) Li, W.; Wojcik, M.; Xu, K. Optical microscopy unveils rapid, reversible electrochemical oxidation and reduction of graphene. *Nano Lett.* **2019**, *19*, 983−989.
(31) Li, Y.; Li, W.; Wojcik, M.; Wang, B.; Lin, L.-C.; Raschke, M. B.; Xu, K. Light-assisted diazonium functionalization of graphene and spatial heterogeneities in reactivity. *J. Phys. Chem. Lett.* **2019**, *10*, 4788−4793.
(32) Li, W.; Li, Y.; Xu, K. Facile, electrochemical chlorination of graphene from an aqueous NaCl solution. *Nano Lett.* **2021**, *21*, 1150−1155.
(33) Cao, P. G.; Xu, K.; Varghese, J. O.; Heath, J. R. Atomic force microscopy characterization of room-temperature adlayers of small organic molecules through graphene templating. *J. Am. Chem. Soc.* **2011**, *133*, 2334−2337.
(34) Cao, P. G.; Xu, K.; Varghese, J. O.; Heath, J. R. The microscopic structure of adsorbed water on hydrophobic surfaces under ambient conditions. *Nano Lett.* **2011**, *11*, 5581−5586.
(35) Vasu, K. S.; Prestat, E.; Abraham, J.; Dix, J.; Kashtiban, R. J.; Beheshtian, J.; Sloan, J.; Carbone, P.; Neek-Amal, M.; Haigh, S. J.; Geim, A. K.; Nair, R. R. Van der Waals pressure and its effect on trapped interlayer molecules. *Nat. Commun.* **2016**, *7*, 12168.
(36) Coleman, V. A.; Knut, R.; Karis, O.; Grennberg, H.; Jansson, U.; Quinlan, R.; Holloway, B. C.; Sanyal, B.; Eriksson, O. Defect formation in graphene nanosheets by acid treatment: an x-ray absorption spectroscopy and density functional theory study. *J. Phys. D-Appl. Phys.* **2008**, *41*, 062001.
(37) Bouleghlimat, E.; Davies, P. R.; Davies, R. J.; Howarth, R.; Kulhavy, J.; Morgan, D. J. The effect of acid treatment on the surface chemistry and topography of graphite. *Carbon* **2013**, *61*, 124−133.
(38) Kim, S. J.; Park, S. J.; Kim, H. Y.; Jang, G. S.; Park, D. J.; Park, J.-Y.; Lee, S.; Ahn, Y. H. Characterization of chemical doping of graphene by in-situ Raman spectroscopy. *Appl. Phys. Lett.* **2016**, *108*, 203111.
(39) Ahn, G.; Ryu, S. Reversible sulfuric acid doping of graphene probed by in-situ multi-wavelength Raman spectroscopy. *Carbon* **2018**, *138*, 257−263.
(40) Hong, Y.; Wang, S.; Li, Q.; Song, X.; Wang, Z.; Zhang, X.; Besenbacher, F.; Dong, M. Interfacial icelike water local doping of graphene. *Nanoscale* **2019**, *11*, 19334−19340.
(41) Liang, X.; Sperling, B. A.; Calizo, I.; Cheng, G.; Hacker, C. A.; Zhang, Q.; Obeng, Y.; Yan, K.; Peng, H.; Li, Q.; Zhu, X.; Yuan, H.; Hight Walker, A. R.; Liu, Z.; Peng, L.-m.; Richter, C. A. Toward Clean and Crackless Transfer of Graphene. *ACS Nano* **2011**, *5*, 9144−9153.
(42) Li, W.; Li, Y.; Xu, K. Azidated graphene: direct azidation from monolayers, click chemistry, and bulk production from graphite. *Nano Lett.* **2020**, *20*, 534−539.
(43) Yeh, P. *Optical Waves in Layered Media*; Wiley: Hoboken, NJ, 2005.

https://doi.org/10.1021/acsnano.1c11616
ACS Nano XXXX, XXX, XXX−XXX